TRACKING INFLUENZA A VIRUS INFECTION IN THE LUNG FROM HEMATOLOGICAL DATA WITH MACHINE LEARNING

Suneet Singh Jhutty[1,2,#], Julia D. Boehme[3,4,#,] Andreas Jeron[3,4], Julia Volckmar[3,4], Kristin Schultz[3,5], Jens Schreiber[6], Klaus Schughart[5, 7,8], Kai Zhou[1], Jan Steinheimer[1], Horst Stöcker[1,9,10], Sabine Stegemann-Koniszewski[6], Dunja Bruder[4,3*], Esteban A. Hernandez-Vargas[1,11*]

1) Frankfurt Institute for Advanced Studies, 60438, Frankfurt am Main, Germany
2) Faculty of Biological Sciences, Goethe University, 60438 Frankfurt am Main, Germany
3) Immune Regulation Group, Helmholtz Centre for Infection Research, 38124 Braunschweig, Germany
4) Infection Immunology Group, Institute of Medical Microbiology, Infection Control and Prevention, Health Campus Immunology, Infectiology and Inflammation, Otto-von-Guericke-University Magdeburg, 39120 Magdeburg, Germany
5) Department of Infection Genetics, Helmholtz Centre for Infection Research, 38124 Braunschweig, Germany
6) Department of Pneumology, Health Campus Immunology, Infectiology and Inflammation, Otto-von-Guericke University Magdeburg, 39120 Magdeburg, Germany
7) Department of Microbiology, Immunology, and Biochemistry, University of Tennessee Health Science Center, Memphis, TN 38163, United States
8) University of Veterinary Medicine Hannover, 30559 Hannover, Germany
9) Institut für Theoretische Physik, Goethe Universität Frankfurt, 60438 Frankfurt am Main, Germany
10) GSI Helmholtzzentrum für Schwerionenforschung GmbH, 64291 Darmstadt, Germany
11) Instituto de Matemáticas, Universidad Nacional Autónoma de México, 76230, Juriquilla, México

Contributions

# These authors contributed equally: Suneet Singh Jhutty, Julia D. Boehme

* These authors jointly supervised this work: Dunja Bruder, Esteban A. Hernandez-Vargas

Correspondence to: dunja.bruder@med.ovgu.de, esteban@im.unam.mx

ABSTRACT

The tracking of pathogen burden and host responses with minimal-invasive methods during respiratory infections is central for monitoring disease development and guiding treatment decisions. Utilizing a standardized murine model of respiratory Influenza A virus (IAV) infection, we developed and tested different supervised machine learning models to predict viral burden and immune response markers, *i.e.* cytokines and leukocytes in the lung, from hematological data. We performed independently *in vivo* infection experiments to acquire extensive data for training and testing purposes of the models. We show here that lung viral load, neutrophil counts, cytokines like IFN-γ and IL-6, and other lung infection markers can be predicted from hematological data. Furthermore, feature analysis of the models shows that blood granulocytes and platelets play a crucial role in prediction and are highly involved in the immune response against IAV. The proposed *in silico* tools pave the path towards improved tracking and monitoring of influenza infections and possibly other respiratory infections based on minimal-invasively obtained hematological parameters.

INTRODUCTION

Respiratory infections by influenza (flu) viruses cause 3 to 5 million cases of severe illness every year[1]. Influenza A virus (IAV) is especially severe among high-risk groups like the elderly, infants, pregnant women, and immunocompromised people[2]. Next to its high prevalence in annual epidemics, IAV has led to high mortality during several pandemics including the Spanish flu in 1918 and more recently the swine flu in 2009[3,4]. Generally, the outcome of flu disease highly depends on viral factors as well as host immunity. Accordingly, a fatal course of infection can result from either insufficient control of viral spread, hyperinflammation, and/or a secondary bacterial infection[5]. Thus, tracking of viral burden as well as host responses in the lungs is important for monitoring IAV pathogenesis and tailoring targeted therapies.

Methodologically, diagnosis and tracking of acute IAV infection can be performed by assessing viral antigen, nucleic acid, or infectious particles from upper or lower airway lavages, aspirates, or swabs. Likewise, monitoring of lower airway immune responses is accomplished by *e.g.* quantification of inflammatory cytokines or leukocytes in bronchoalveolar lavage fluid (BALF). Next to several obvious disadvantages of these methods (low sensitivity, costly and time-consuming analyses, and/or high technical requirements), the biggest hurdle lies in the invasive sampling procedure that poses a risk to the acutely infected patient[6]. Accordingly, the development of non- or minimally invasive approaches that allow observation of the disease status during IAV infection remains an unmet medical need.

Besides inducing acute inflammatory responses in the airways, influenza infection results in peripheral immune activation manifesting in altered blood cell composition[7], transcriptional signatures, and cytokine and chemokine levels in mice and humans[8–10]. While the severity and longitudinal analyses revealed distinct molecular and/or cellular characteristics in peripheral blood

of IAV infected hosts, the suitability of each of these markers (and blood parameters in general) for predicting the disease status is still unknown.

Here, we propose for the first time a framework intertwining *in vivo* experiments and machine learning methods to forecast IAV infection parameters in the lung from blood sample data that can be accessed minimal-invasively. To this end, we employed different machine-learning models for blood-lung mapping. Experimentally, we utilized an established mouse model of sublethal respiratory IAV infection[11,12] and simultaneously assessed the kinetics of pathogen burden, lung inflammation, as well as systemic cellular changes following infection. Ultimately, several independent *in vivo* experiments were used to validate the applicability of the proposed framework. Our primary computational approach was deep learning, which represents a class of machine learning algorithms that uses multiple layers of information processing for feature extraction and pattern analysis[13,14]. These methods have already been successfully applied in several biological fields including the prediction of transcriptional enhancers[15], protein secondary structure[14], and the pathogenicity of genetic variants[17]. The image recognition abilities of machine learning algorithms have already been tested for their diagnostic value and show promising results[18,19].

RESULTS

Our methodology consisted of three consecutive stages: *in vivo* experimental data acquisition, model training, and independent experimental model validation (Figure 1). For the acquisition of experimental data, mice were infected with a sublethal dose of PR8 (H1N1) followed by the quantification of lung viral load, pulmonary innate and adaptive leukocyte subsets, pulmonary cytokine levels, and hematological parameters over a total period of 11 days. Blood and lung parameters were measured (Figure 1) in two independent experiments, mice (n = 4-6 per time point) were sacrificed on days 1, 2, 3, 4, 5, 7, 9, and 11 post-infection (pi). These experimental data built the basis for model training using different machine learning approaches to identify the relationship between hematological and pulmonary parameters and to train and optimize the model accordingly. To validate the predictive value of our model, we performed two additional independent infection experiments with mice sacrificed on days 2, 4, 6, 9, and 11 pi and used the mathematical models to predict the lung viral burden, leukocyte composition, and cytokine levels, respectively, based on experimental hematological parameters.

Blood and Lung Data Analysis. In a first step, we conducted a correlation analysis to uncover potential linear relationships between selected hematological and pulmonary parameters (Figure 2 and Supplementary Figures S10-12). We found a very strong correlation (Pearson correlation coefficient > 0.9) between blood leukocytes and lymphocytes, which can be attributed to the fact that lymphocytes constitute the largest leukocyte fraction in mice[20]. Likewise, a strong correlation observed between hematocrit as well as hemoglobin and erythrocyte numbers (Pearson correlation coefficient > 0.8) can be attributed to the fact that hematocrit, as well as hemoglobin, are red blood cell-associated parameters[21].

Strikingly, we did not observe any strong correlation between blood and lung compartment variables. However, there were strong correlations within cells of the lung compartment, such as $CD4^+$ T cells and $CD8^+$ T cells as well as neutrophils and natural killer (NK) cells. As a linear correlation does not include higher-order nonlinear temporal relations, we next employed machine learning algorithms and compared the obtained results with the linear regression model.

Tracking IAV Infection in the Lungs from Blood-Derived Parameters. To predict influenza virus levels and immunological markers in the lungs from hematological parameters, we employed feedforward neural networks, gradient boosted regression trees, and a linear regression model. These algorithms considered 14 hematological parameters (see Table 1) as features to predict the respective target lung variable. The main scores used for comparing and evaluating different machine learning algorithms were based on the average squared difference between the estimated values and the actual value (mean squared error). The proportion of the variance in the dependent variable that is predictable from the independent variables was based on the R^2 score. Overfitting was reduced with regularization techniques presented in methods.

Figure 3A illustrates the best model prediction of viral levels in the lung, *i.e.* the feedforward neural network, based on experimental haematological data. We observed that the model had a good qualitative behavior of the lung viral load (measured as copy numbers of NP transcripts) over the experimental time-frame of eleven days. Day 0 represents the control group. The prediction seemed to be most accurate around the peak of viral replication, *i.e.* days 4 and 5 pi. Quantitatively, there was a high variation in the predictions. This was attributed to the variation found in our infection experiments (Figure S1-S9), which is a common observation *in vitro* and *in vivo* viral infection experiments[22–27]. While for some animals there was a large difference between the actual

141 experimental data and the respective predictions in the testing experiments, overall, the qualitative
142 performance on the testing set was good (Figure 3B).

143 In addition to predicting the lung viral load, we tested several machine learning algorithms to
144 predict target lung leukocytes and cytokines from the hematological parameters (Table 2). The
145 comparison in Figure 4A shows how the respective best model performed for different targets (for
146 all results please refer to the supplemental material, Supplementary Figures S13-15). As a
147 benchmark, we used the mean for each target variable calculated from the training data. In almost
148 all cases, the best model performed better than the benchmark. A positive R^2 score demonstrates
149 the explanatory power of the model. Predictions for lung IFN-γ, viral load, IL-6, and neutrophils
150 were able to outperform the benchmark (Figure 4). Predictions for other lung target parameters are
151 presented in Supplementary Figure S13-S15. Notably, the accuracy of the model predictions was
152 dependent on the stage of the infection. For example, neutrophil numbers in the lungs were better
153 predicted in the later days of infection, while IL-6 and IFN-γ levels were more accurately predicted
154 at the peak of infection (Figure 4B-D). This was also observed for other immune cells such as
155 $CD4^+$ and $CD8^+$ T cells (Figure S13). Table 2 presents a summary of the best models for predicting
156 the different lung target parameters.

157 To determine the role of each feature from the hematological data for the prediction of lung
158 outcomes, we performed a feature importance analysis. For this, we calculated the permutation
159 importance by swapping out features and evaluating the performance of our testing data. The
160 results of the feature importance analysis are organized from top to bottom in the level of
161 importance in Figure 5. For example, from all hematological parameters, granulocytes showed the
162 greatest impact on the performance of the machine learning models for predicting the viral load,

neutrophils, IFN-γ, and IL-6. Interestingly our analyses revealed a pivotal role of blood platelets for predicting both pathogen burden and lung inflammatory milieu (Figure 5). Granulocytes and erythrocytes ranked second and third place, respectively. The feature importance plots of the additional lung target immune cells and cytokines can be found in the supplemental material (Figure S16).

DISCUSSION

Mathematical modeling of host immune responses has largely contributed to improving our understanding of the overall course of influenza infection[28–37] as well as the personalization of therapies and vaccines[38–40]. Mathematical models consist of systems of ordinary differential equations describing the viral dynamics within the host. However, computational tools for the diagnosis and tracking of respiratory diseases remain a public health challenge.

Here, we progress from the state of the art showing for the first time that minimal-invasively acquired haematological parameters can be used to infer lung viral burden, leukocytes, and cytokines following IAV infection in mice. Nevertheless, despite standardized experimental procedures, our analysis showed a large variance in the computational predictions. These can be attributed to the relatively high variances of our experimental data due to biological or experimental variations. For instance, we found differences in some hematological parameters between the training and the testing experiments, which possibly explain the differences in performance between training and testing prediction of the lung viral load for day 2 post-infection.

The clinical potential of the framework proposed here consists of a new qualitative vision of the disease processes in the lung compartment. We show that the accumulation and decline of multiple cell types involved in the anti-viral immune response in the lung can successfully be predicted with data derived from peripheral blood analyses. The boosted regression tree, with some modifications, provided the best results for many of the lung immune target cells. On the other hand, some target variables proved to be difficult to predict from hematological data. For instance, alveolar macrophage (AM) numbers could not be predicted with any of the tested algorithms and showed the worst score. This is likely the result of the weak correlations of AMs with the different

blood cells analyzed. AMs also demonstrate a quite different behavior than the other cells in terms of their abundance over the course of infection as their number peaked rather late during the infection, *i.e.* when the virus was mostly cleared[41]. This phenomenon is most likely the result of inflation of the alveolar macrophage pool by self-renewal[42] and/or monocyte recruitment processes[43]. Regarding the less accurate predictions of cytokines within the airways from blood parameters (Supplementary Figure S13), a possible explanation is that a large portion of these cytokines (especially during the early infection stage) originated from lung-resident leukocytes as well as non-leukocytes. Therefore, their temporal quantity and composition are largely determined by local constituents of the lung´s immune cell response.

Our results show an active reaction chain between peripheral blood parameters and immune cells in the lungs of the mice following IAV infection. Interestingly, we found that peripheral blood platelets play an important role in predicting lung immune cell numbers in IAV infection. In line with our finding of increased numbers of platelets in the blood during the acute phase of IAV infection (see Supplementary Figure S1), platelet accumulation in the pulmonary capillaries is a hallmark of murine IAV H1N1 infection[44] and contributes to pathogenesis[45]. Importantly, platelet-derived cytokines such as IL-1β can directly increase endothelial permeability and the expression of important vascular adhesion molecules[46,47]. In line with this, airway IL-1β levels were elevated during acute IAV infection (see Figures S8-9). Increased platelet-mediated transendothelial migration of $CD4^+$ T cells, $CD8^+$ T cells, NK cells, and neutrophils could thus be one conceivable mechanism contributing to the observed strong positive correlation between peripheral blood platelets and the aforementioned lung leukocyte subsets. This is relevant to the anti-viral host response, as the $CD4^+$ T cells are central in the activation and maturation of virus-specific $CD8^+$ T cells[48], while neutrophils are required for proper NK cell maturation[49].

It should be noted, that although the estimation is called “prediction” in the machine learning domain, and blood-derived data can here be used in a practical way to "predict" the viral load or the number of certain lung immune cells or cytokines in IAV infection, we cannot establish a direction of causality in this case. In other words, we cannot state *e.g.* that platelets are involved in raising the total amount of $CD8^+$ T cells or if $CD8^+$ T cells drive the increase in platelets. What we can learn from the correlations between variables is that $CD8^+$ T cells, $CD4^+$ T cells, NK cells, and neutrophils have their strongest positive correlation with platelets between the blood cells analyzed (see Figure 2). The feature importance analysis confirms that platelets play the most important part in the estimation of lung $CD4^+$ T and $CD8^+$ T cells, followed by erythrocytes. However, the viral load inside the lungs has also a strong correlation with platelets but an even stronger one with granulocytes. The variable importance analysis suggests that platelets and granulocytes do not strongly contribute to the prediction as can be seen in Figure 5.

The weak predictive results obtained with the linear regression model signifies that these relations have a high order of complexity. While contributing to the viral clearance, the innate immune system can also exacerbate the lung injury[50,51]. In this context, tissue injury can be a cause of platelet activation during influenza infection. The role of platelets in human influenza infection has been stressed in recent years[45,52,53]. Thrombosis, controlled by the innate immune system has been suggested to support immune defense[54].

Hematological parameters such as neutrophil, lymphocyte, and platelet counts, as well as the neutrophil-to-lymphocyte ratio (NLR) have contributed to diagnosing influenza virus infections[52]. Thus, we also addressed if the use of the granulocyte-lymphocyte ratio (GLR) or the platelet-granulocyte ratio (PGR) improves importance in our model predictions (Table S2). We compared the use of only GLR or PGR with the only use of lymphocytes and granulocytes, as well using

additional important IAV infection-associated peripheral blood parameters like erythrocytes and hemoglobin. Performances were evaluated with the MSE and R^2 scores on the testing data set. We also calculated the corrected Akaike Information Criterion (AIC_c) during the training to take the complexity of the models into account. Supplementary Table S2 shows that the model performance increased using GLR, while the use of PGR had only a minor effect. Also, adding erythrocytes and hemoglobin did not improve predictions.

In summary, blood platelets, granulocytes, and erythrocytes play an important role in understanding the immune response to influenza infection and can be used in conjunction with other blood components for monitoring the lung viral load and lung immune cells in mice. Importantly, our results indicate that a reduced number of variables does not affect model/prediction accuracy. This can help to further reduce the hematology data needed for successful prediction. While recent efforts show evidence for the diagnosis of COVID-19 from blood compartment[56], further clinical evidence will be needed to show the potential of how our procedure could be generalized to advance medical care.

METHODS

Experimental Design. Mice were intranasally infected with a sublethal dose of the mouse-adapted, strictly pneumotropic H1N1 IAV strain PR/8/34 and the lung viral burden, pulmonary innate and adaptive leukocyte subsets, pulmonary cytokine levels, and peripheral blood cell parameters were assessed for 11 days pi (Figure 1).

Initial generation, training, and optimization of the computational algorithms were conducted using data from two independent *in vivo* infection experiments. Here, mice were randomly assigned to the respective experimental groups and were either intranasally inoculated with a sublethal dose of IAV or saline (control groups). Mice (n = 4-6/experimental group) were sacrificed on days 1, 2, 3, 4, 5, 7, 9 and 11 post-infection. Experimental readouts for the first experiment were: hematological parameters and lung tissue viral load. In the second experiment, experimental readouts were: hematological parameters, leukocytes in lung tissue, and airway cytokines.

For subsequent model validation, two additional, independent *in vivo* infection experiments were performed using the above-mentioned readouts. In these experiments, mice (n = 3/experimental group) were sacrificed at days 2, 4, 6, 9, and 11 post-infection. Hematological parameters used for model generation and evaluation are listed in Table 1.

Mice. For all experiments, female C57BL/6JOlaHsd mice (age 10-12 weeks) from Envigo were used. All mice were housed in the animal facility at the Helmholtz Centre for Infection Research under specific-pathogen-free (SPF) conditions and in accordance with national and institutional guidelines.

Viral preparation and infection. For viral infections, a mouse-adapted influenza A virus strain (A/Puerto Rico/8/34, H1N1) was utilized. The virus was produced in Madin-Darby Canine Kidney

(MDCK) cells[57] and quantified by calculating the tissue culture infectious dose (TCID50) as previously described[58]. Mice were anesthetized by intraperitoneal injection of ketamine/xylazine and were infected with viral inoculum (0.31 TCID50 in 25µL PBS). Control animals received PBS only.

Quantification of the lung viral load. Lungs were perfused using PBS. RNA was extracted from whole lung tissue homogenates using the RNeasy Plus Mini Kit (Qiagen). The absence of genomic DNA in RNA samples was initially confirmed by PCR using a Taq DNA-polymerase and primers for the housekeeping gene Rps9. Quantitative real-time RT-PCR (qPCR) for detection of viral burden was performed using the SensiFASTTM SYBR® No-ROX One-Step Kit and an influenza nucpleoprotein (NP) plasmid standard. The sequences of the used primers were: 5′ CTGGACGAGGGCAAGATGAAGC, 3′ TGACGTTGGCGGATGAGCACA (*Rps9*) and 5′ GAGGGGTGAGAATGGACGAAAAAC, 3′ CAGGCAGGCAGGCAGGACTT (*Np*).

Hematology analysis. Blood samples were obtained from the retrobulbar plexus and EDTA was added to prevent coagulation. Samples were analyzed using a VetScan® HM5 machine (Abaxis).

Cytokine detection. Bronchoalveolar lavage (BAL) was performed with 1mL PBS, samples were spun down (420 x g, 10 min) and BAL fluid (BALF) supernatants were stored at -70°C until further analyses. Cytokine levels in BALF samples were quantified using the LEGENDplex™ Mouse Inflammation Panel (BioLegend) according to the manufacturer's protocol.

Isolation of leukocytes from lung tissue. Lungs were perfused using PBS, excised, mechanically homogenized, and enzymatic digestion was performed in Iscove's modified Dulbecco's medium (IMDM) supplemented with 0.2mg/mL collagenase D (Roche), 0.01mg/mL DNase I (Sigma-

Aldrich), and 5% fetal bovine serum at 37°C for 45min. Digestion was stopped by the addition of EDTA, the cell suspension was filtered through a 100µm cell strainer and spun down (420 x g, 10min). Erythrocyte lysis was performed using ammonium-chloride-potassium (ACK) buffer and leukocytes were isolated by gradient centrifugation using Percoll solution (GE Healthcare). Lung tissue leukocytes were filtered again and antibody staining for flow cytometry was performed.

Flow cytometry. Lung tissue leukocyte samples were subjected to viability staining and blocking of Fc-receptors using LIVE/DEAD™ Fixable Blue Dead cell stain kit (life technologies) and an anti-CD16/32 antibody (clone 93, BioLegend). Cells were then washed and incubated with a staining mix containing antibodies against the following murine antigens: Siglec-F (PE, clone E50-2440, BD), Ly6G (AlexaFluor700, clone 1A8, BD), CD11c (APC, clone N 418, BioLegend), CD11b (BV421, clone M1/70, BD), CD4 (APC-Fire750, clone GK1.5, BioLegend), CD8a (CyChrome, clone 53-6.7, BD), CD3ε (Biotin, clone 145-2C11, BioLegend), NK1.1 (FITC, clone PK136, BioLegend). Secondary staining was performed using streptavidin-BV605 and streptavidin-BV650, respectively (BioLegend). All reagents and antibodies had been titrated before the experiments for optimal staining results. Flow cytometry data were acquired using LSRII and LSR Fortessa instruments (BD). Data were analyzed using FlowJo software (BD).

Data Processing. The data obtained from the hematological analysis constitutes of 20 different parameters. Some parameters are given in absolute values and percentages. We considered from these parameters only the absolute values, resulting in 14 different parameters (see Table 1). For some mice, it was not possible to extract hematological data and/or according to target infection marker. These mice were removed for the mapping, although their data was used in the correlation analysis. Furthermore, if some values were lower than the measurable threshold, we used the threshold value. Computational algorithms were implemented in python using the *Keras* and

sklearn libraries. Our study design yielded separate training and testing data sets. The testing data was obtained approximately one year after the training data. All laboratory conditions were kept as similar as possible.

Using the data directly for training the algorithms led to poor results and therefore we used data pre-processing techniques. To conserve the nature of hematological parameter distributions, we used the min-max scaling from the sklearn.preprocessing. MinMaxScaler class:

$$z = \frac{x - x_{min}}{x_{max} - x_{min}}$$

For the target infection markers like viral load, any logarithmic function worked well. For simplicity, we used $\log_{10}$.

Machine Learning Models. Different machine learning models were tested for the mapping including feedforward neural networks (FNN), gradient boosted regression trees (GBRT), linear regression (LR), support vector machines (SVM), and random forest regression (RFR). The hyperparameters of the models were estimated via grid-search and adjusted via trial and error. FNN and GBRT showed to superior in most cases and RFR was outperformed in every instance with one of the other algorithms.

In many cases using PCA before the mapping yielded improved performance. It was found that a dimensionality reduction to six input blood variables was often best. We used the class *sklearn.decomposition.PCA* for implementation. For the feedforward neural network, the *keras* library was used with a TensorFlow backend. We found that one hidden layer was sufficient most of the time and additional layers were not needed. The number of weights varied from 10 to 50. For regularization, the addition of dropout layers with a rate of 0.2 was helpful to prevent

355 overfitting. As an activation function, we used a rectified linear unit (ReLU). We had one output
356 that uses a linear activation function. This was necessary to map the whole range of possible
357 outcome values. We used the Adam optimizer and minimized the mean squared error to find the
358 optimal fit. The weights were initialized according to a He-uniform distribution.[59] Following
359 common practice in literature we used for the training of the neural network a validation set of
360 10% of the whole training data.

361 The GBRT, LR, SVM, and RFR algorithms are taken from the python library *sklearn*. The
362 hyperparameters of GBRT and RFR models were searched over a grid from 10 to 2000 estimators,
363 a learning rate from 0.001 to 0.09, and a max depth of 2 to 14. The least-square regression was
364 used for optimization. The kernels used for SVM were *'linear'*, *'poly'*, *'rbf '*, *'sigmoid'* and
365 *'precomputed'*.

366 To determine which variables were the most important in our model predictions, we calculated the
367 permutation importance using the sklearn.inspection.permutation_importance implementation.
368 For this, we took our best model, respectively, and trained it on the training data set. After the
369 trained model was evaluated on the hold-out testing data set with the mean squared error as metric,
370 a feature column was permuted and the metric was evaluated again. This procedure was repeated
371 100 times and the permutation importance was given by the difference between the baseline metric
372 and the metric from permutated feature columns.

373 ## DATA AND CODE AVAILABILITY

374 The datasets generated and analyzed during the current study are available:

375 https://github.com/Jhutty/Tracking_IAV_from_Blood

376

REFERENCES

1. World Health Organization. Influenza (Seasonal) fact sheet.
2. WHO Recommended Surveillance Standards. Second edition.
3. Kilbourne, E. D. Influenza Pandemics of the 20th Century. *Emerging Infectious Diseases* **12**, 9 (2006).
4. World Health Organization. Writing Committee of the WHO Consultation on Clinical aspects of pandemic 2009 influenza A (H1N1) virus infection. *New England Journal of Medicine* 1708–1719 (2010).
5. Sharma-Chawla, N. *et al.* In vivo neutralization of pro-inflammatory cytokines during secondary streptococcus pneumoniae infection post influenza a virus infection. *Frontiers in Immunology* **10**, (2019).
6. Allwinn, R. *et al.* Laboratory diagnosis of influenza – virology or serology? *Medical Microbiology and Immunology 2002 191:3* **191**, 157–160 (2002).
7. L, D. *et al.* Cellular changes in blood indicate severe respiratory disease during influenza infections in mice. *PloS one* **9**, (2014).
8. IE, G. *et al.* Untuned antiviral immunity in COVID-19 revealed by temporal type I/III interferon patterns and flu comparison. *Nature immunology* **22**, 32–40 (2021).
9. Y, Z. *et al.* Pathway mapping of leukocyte transcriptome in influenza patients reveals distinct pathogenic mechanisms associated with progression to severe infection. *BMC medical genomics* **13**, (2020).
10. BM, C. *et al.* Inflammatory Monocytes Drive Influenza A Virus-Mediated Lung Injury in Juvenile Mice. *Journal of immunology (Baltimore, Md. : 1950)* **200**, 2391–2404 (2018).
11. N, S.-C. *et al.* Influenza A Virus Infection Predisposes Hosts to Secondary Infection with Different Streptococcus pneumoniae Serotypes with Similar Outcome but Serotype-Specific Manifestation. *Infection and immunity* **84**, 3445–3457 (2016).
12. Duvigneau, S. *et al.* Hierarchical effects of pro-inflammatory cytokines on the post-influenza susceptibility to pneumococcal coinfection. *Scientific Reports* **6**, 1–11 (2016).
13. Ian Goodfellow, Yoshua Bengio & Aaron Courville. Deep learning. *MIT press* (2016) doi:10.1007/S10710-017-9314-Z.
14. DengLi & YuDong. Deep Learning. *Foundations and Trends in Signal Processing* **7**, 197–387 (2014).
15. Liu, F., Li, H., Ren, C., Bo, X. & Shu, W. PEDLA: predicting enhancers with a deep learning-based algorithmic framework. *Scientific Reports 2016 6:1* **6**, 1–14 (2016).
16. Wang, S., Peng, J., Ma, J. & Xu, J. Protein Secondary Structure Prediction Using Deep Convolutional Neural Fields. *Scientific Reports 2016 6:1* **6**, 1–11 (2016).

17. Quang, D., Chen, Y. & Xie, X. DANN: a deep learning approach for annotating the pathogenicity of genetic variants. *Bioinformatics* **31**, 761–763 (2015).

18. Esteva, A. *et al.* Dermatologist-level classification of skin cancer with deep neural networks. *Nature 2017 542:7639* **542**, 115–118 (2017).

19. Huang, Q., Zhang, F. & Li, X. Machine Learning in Ultrasound Computer-Aided Diagnostic Systems: A Survey. *BioMed Research International* **2018**, (2018).

20. Kabak, M., Çil, B. & Hocanlı, I. Relationship between leukocyte, neutrophil, lymphocyte, platelet counts, and neutrophil to lymphocyte ratio and polymerase chain reaction positivity. *International Immunopharmacology* **93**, 107390 (2021).

21. Han, Q. *et al.* Role of hematological parameters in the diagnosis of influenza virus infection in patients with respiratory tract infection symptoms. *Journal of Clinical Laboratory Analysis* **34**, e23191 (2020).

22. Hernandez-Vargas, E. A. *et al.* Effects of Aging on Influenza Virus Infection Dynamics. *Journal of Virology* **88**, 4123–4131 (2014).

23. Hernandez-Vargas, E. A. & Velasco-Hernandez, J. X. In-host Mathematical Modelling of COVID-19 in Humans. *Annual Reviews in Control* **50**, 448–456 (2020).

24. Pawelek, K. A. *et al.* Modeling Within-Host Dynamics of Influenza Virus Infection Including Immune Responses. *PLOS Computational Biology* **8**, e1002588 (2012).

25. Dobrovolny, H. M., Gieschke, R., Davies, B. E., Jumbe, N. L. & Beauchemin, C. A. A. Neuraminidase inhibitors for treatment of human and avian strain influenza: A comparative modeling study. *Journal of Theoretical Biology* **269**, 234–244 (2011).

26. Baccam, P., Beauchemin, C., Macken, C. A., Hayden, F. G. & Perelson, A. S. Kinetics of Influenza A Virus Infection in Humans. *Journal of Virology* **80**, 7590–7599 (2006).

27. Smith, A. M. *et al.* Kinetics of Coinfection with Influenza A Virus and Streptococcus pneumoniae. *PLOS Pathogens* **9**, e1003238 (2013).

28. Miao, H., Xia, X., Perelson, A. S. & Wu, H. On Identifiability of Nonlinear ODE Models and Applications in Viral Dynamics. *SIAM Review* **53**, 3–39 (2011).

29. Canini, L. & Perelson, A. S. Viral kinetic modeling: state of the art. *Journal of Pharmacokinetics and Pharmacodynamics* **41**, 431–443 (2014).

30. Canini, L. & Carrat, F. Population modeling of influenza A/H1N1 virus kinetics and symptom dynamics. *Journal of Virology* **85**, 2764–2770 (2011).

31. Handel, A. & Antia, R. A simple mathematical model helps to explain the immunodominance of CD8 T cells in influenza A virus infections. *Journal of virology* **82**, 7768–72 (2008).

32. Beauchemin, C. & Handel, A. A review of mathematical models of influenza A infections within a host or cell culture: lessons learned and challenges ahead. *BMC public health* **11**, S7 (2011).

33. Hancioglu, B., Swigon, D. & Clermont, G. A dynamical model of human immune response to influenza A virus infection. *Journal of Theoretical Biology* **246**, 70–86 (2007).

34. Smith, A. M. Host-pathogen kinetics during influenza infection and coinfection: insights from predictive modeling. *Immunological Reviews* vol. 285 97–112 (2018).

35. Smith, A. M. & Perelson, A. S. Influenza A virus infection kinetics: quantitative data and models. *Wiley interdisciplinary reviews. Systems biology and medicine* **3**, 429–445 (2011).

36. Baccam, P., Beauchemin, C., Macken, C. a, Hayden, F. G. & Perelson, A. S. Kinetics of influenza A virus infection in humans. *Journal of virology* **80**, 7590–9 (2006).

37. Harper, S. A. *et al.* Seasonal Influenza in Adults and Children—Diagnosis, Treatment, Chemoprophylaxis, and Institutional Outbreak Management: Clinical Practice Guidelines of the Infectious Diseases Society of America. *Clinical Infectious Diseases* **48**, 1003–1032 (2009).

38. Hernandez-Mejia, G. & Hernandez-Vargas, E. A. Uncovering antibody cross-reaction dynamics in influenza A infections. *bioRxiv* 2020.01.06.896274 (2020) doi:10.1101/2020.01.06.896274.

39. Hernandez-Mejia, G., Alanis, A. Y. & Hernandez-Vargas, E. A. Inverse Optimal Impulsive Control Based Treatment of Influenza Infection. in *IFAC World Congress 2017* vol. 50 12696–12701 (2017).

40. Parra-Rojas, C., Messling, V. & Hernandez-Vargas, E. A. Adjuvanted influenza vaccine dynamics. *Scientific Reports* **9**, (2019).

41. Toapanta, F. R. & Ross, T. M. Impaired immune responses in the lungs of aged mice following influenza infection. *Respiratory Research* **10**, 1–19 (2009).

42. Yao, Y. *et al.* Induction of Autonomous Memory Alveolar Macrophages Requires T Cell Help and Is Critical to Trained Immunity. *Cell* **175**, 1634-1650.e17 (2018).

43. Aegerter, H. *et al.* Influenza-induced monocyte-derived alveolar macrophages confer prolonged antibacterial protection. *Nature immunology* **21**, 145–157 (2020).

44. Rommel, M. G. E., Milde, C., Eberle, R., Schulze, H. & Modlich, U. Endothelial–platelet interactions in influenza-induced pneumonia: A potential therapeutic target. *Anatomia, Histologia, Embryologia* **49**, 606–619 (2020).

45. Lê, V. B. *et al.* Platelet Activation and Aggregation Promote Lung Inflammation and Influenza Virus Pathogenesis. *https://doi.org/10.1164/rccm.201406-1031OC* **191**, 804–819 (2015).

46. Rossaint, J., Margraf, A. & Zarbock, A. Role of Platelets in Leukocyte Recruitment and Resolution of Inflammation. *Frontiers in Immunology* **0**, 2712 (2018).

47. Hawrylowicz, C. M., Howells, G. L. & Feldmann, M. Platelet-derived interleukin 1 induces human endothelial adhesion molecule expression and cytokine production. *Journal of Experimental Medicine* **174**, 785–790 (1991).

48. Zens, K. D. & Farber, D. L. Memory CD4 T Cells in Influenza. *Current Topics in Microbiology and Immunology* **386**, 399–421 (2014).

49. Jaeger, B. N. *et al.* Neutrophil depletion impairs natural killer cell maturation, function, and homeostasis. *Journal of Experimental Medicine* **209**, 565–580 (2012).

50. Herold, S., Becker, C., Ridge, K. M. & Budinger, G. R. S. Influenza virus-induced lung injury: pathogenesis and implications for treatment. *European Respiratory Journal* **45**, 1463–1478 (2015).

51. Kuiken, T., Riteau, B., Fouchier, R. A. M. & Rimmelzwaan, G. F. Pathogenesis of influenza virus infections: the good, the bad and the ugly. *Current Opinion in Virology* **2**, 276–286 (2012).

52. Koupenova, M. *et al.* The role of platelets in mediating a response to human influenza infection. *Nature Communications 2019 10:1* **10**, 1–18 (2019).

53. Assinger, A. Platelets and Infection – An Emerging Role of Platelets in Viral Infection. *Frontiers in Immunology* **0**, 649 (2014).

54. Engelmann, B. & Massberg, S. Thrombosis as an intravascular effector of innate immunity. *Nature Reviews Immunology 2012 13:1* **13**, 34–45 (2012).

55. Han, Q. *et al.* Role of hematological parameters in the diagnosis of influenza virus infection in patients with respiratory tract infection symptoms. *Journal of Clinical Laboratory Analysis* **34**, e23191 (2020).

56. Kukar, M. *et al.* COVID-19 diagnosis by routine blood tests using machine learning. *Scientific Reports 2021 11:1* **11**, 1–9 (2021).

57. Stegemann, S. *et al.* Increased Susceptibility for Superinfection with Streptococcus pneumoniae during Influenza Virus Infection Is Not Caused by TLR7-Mediated Lymphopenia. (2009) doi:10.1371/journal.pone.0004840.

58. REED, L. J. & MUENCH, H. A SIMPLE METHOD OF ESTIMATING FIFTY PER CENT ENDPOINTS. *American Journal of Epidemiology* **27**, 493–497 (1938).

59. He, K., Zhang, X., Ren, S. & Sun, J. Delving Deep into Rectifiers: Surpassing Human-Level Performance on ImageNet Classification.

ACKNOWLEDGEMENTS

We thank Tatjana Hirsch, Hanna Shkarlet and Karin Lammert for expert technical assistance in infection experiments. This work was supported by the Deutsche Forschungsgemeinschaft with the project HE7707/5-1 and BR2221/6-1; the Universidad Nacional Autonoma de Mexico (UNAM) – PAPIIT with the number IA102521; and the Alfons und Gertrud Kassel-Stiftung.

ETHICS DECLARATIONS

All the experiments were approved and conducted in accordance with the guidelines set by the local animal welfare and ethics committee (Niedersächsisches Landesamt für Verbraucherschutz und Lebensmittelsicherheit).

COMPETING INTERESTS

The authors declare no competing interests.

FIGURES

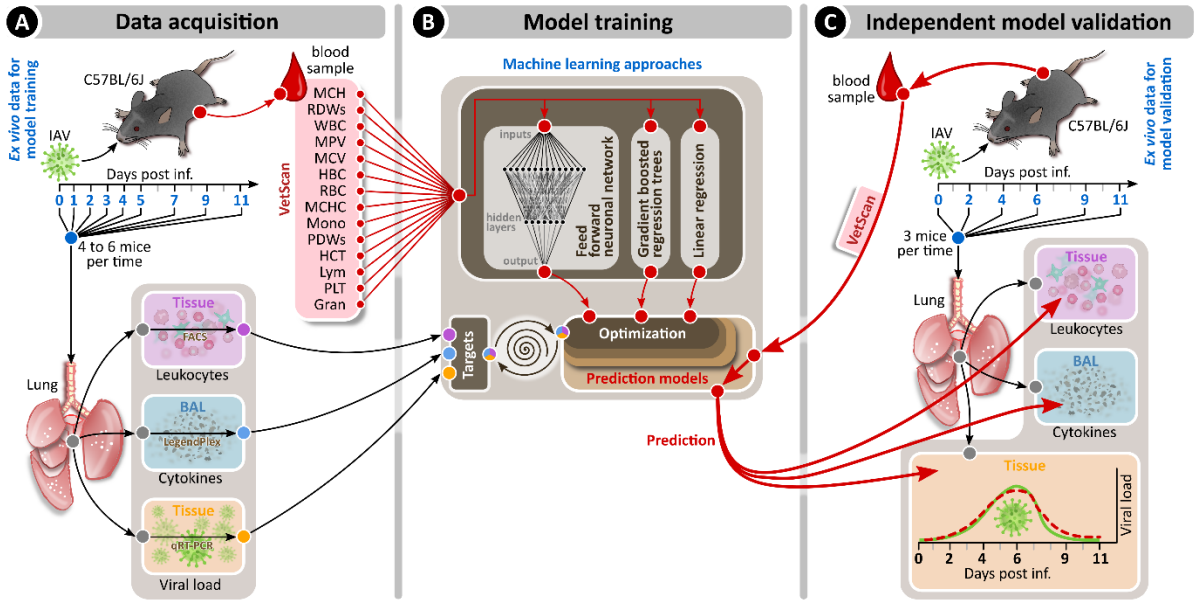

Figure 1: Experimental scheme for the machine learning approaches of the respiratory IAV infection. Mice were intranasally infected with a sublethal dose of IAV PR/8/34 on day 0 and sacrificed on the indicated days. Blood was collected for hematology analyses (Supplementary Figures S1-2), bronchoalveolar lavage was performed to analyze lung cytokines and lung tissue samples were used to monitor either viral load (experiment 1, Supplementary Figure S5) or pulmonary leukocyte subsets (experiment 2, Supplementary Figures S6, S8) (A). The hematological data from this initial set of experiments were used to build and train different machine learning models (B). Data from a separate experiment (Supplementary Figures S3-5, S7, S9) were used for testing and evaluation of machine learning algorithms (C).

A)

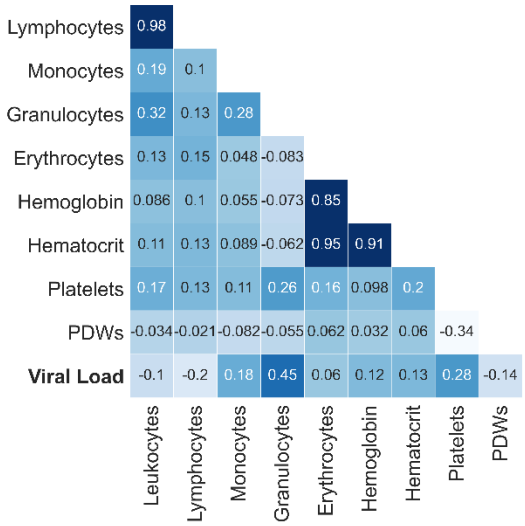

B)

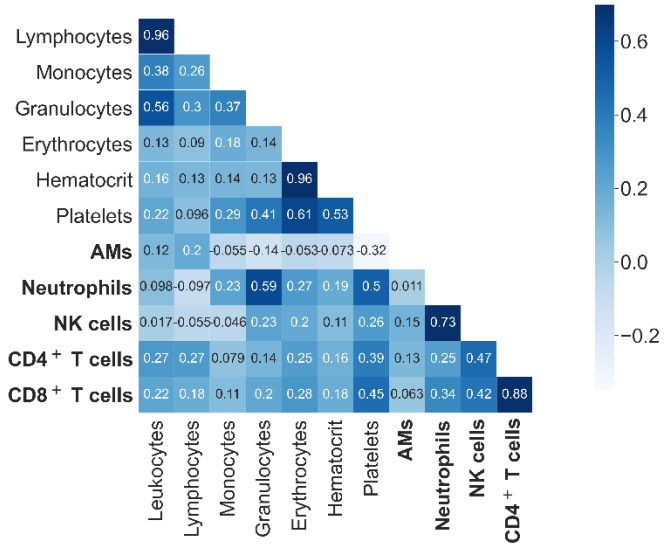

Figure 2. Selected correlations of blood cells, lung leukocytes, and lung viral load for influenza infection. (A) shows the correlation of blood cells with lung viral load. (B) shows the correlation of blood cells with lung leukocytes. The matrices depict the respective Pearson correlation coefficients from the initial experiments used as training data for the machine learning models. We observed some strongly related clusters like erythrocytes, haemoglobin, and hematocrit or NK, $CD4^+$ T, and $CD8^+$ T cells. IAV-associated lung markers that were later predicted are shown in bold letters. All other parameters were provided to the algorithm to make the estimation. Here, only a small subset of the data and its correlations are shown. To view all the data with its correlations, please refer to the supplemental material (Supplementary Figures S10-12).

A)

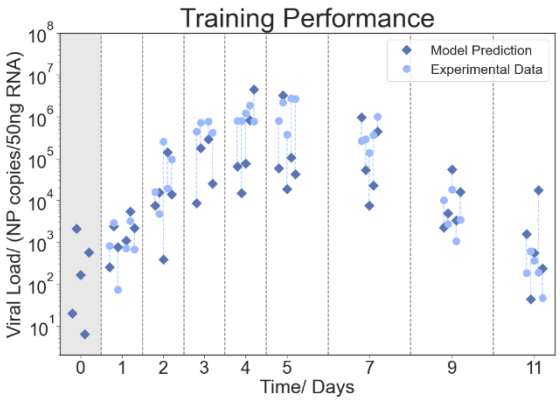

B)

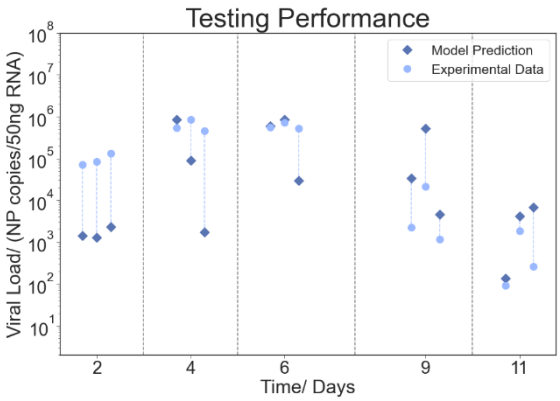

Figure 3. Mapping of the lung viral load from blood data. The plots show the training and testing performance of the neural network model. (A) shows the performance of the model on the training data. (B) shows the performance of the testing data obtained from a second experiment. Each circle represents one mouse, with its matching individual prediction indicated by a connected (blue dashed line) diamond. The vertical lines divide experimental days. Day 0 marks the control group (viral load below measurable threshold) and is highlighted in grey.

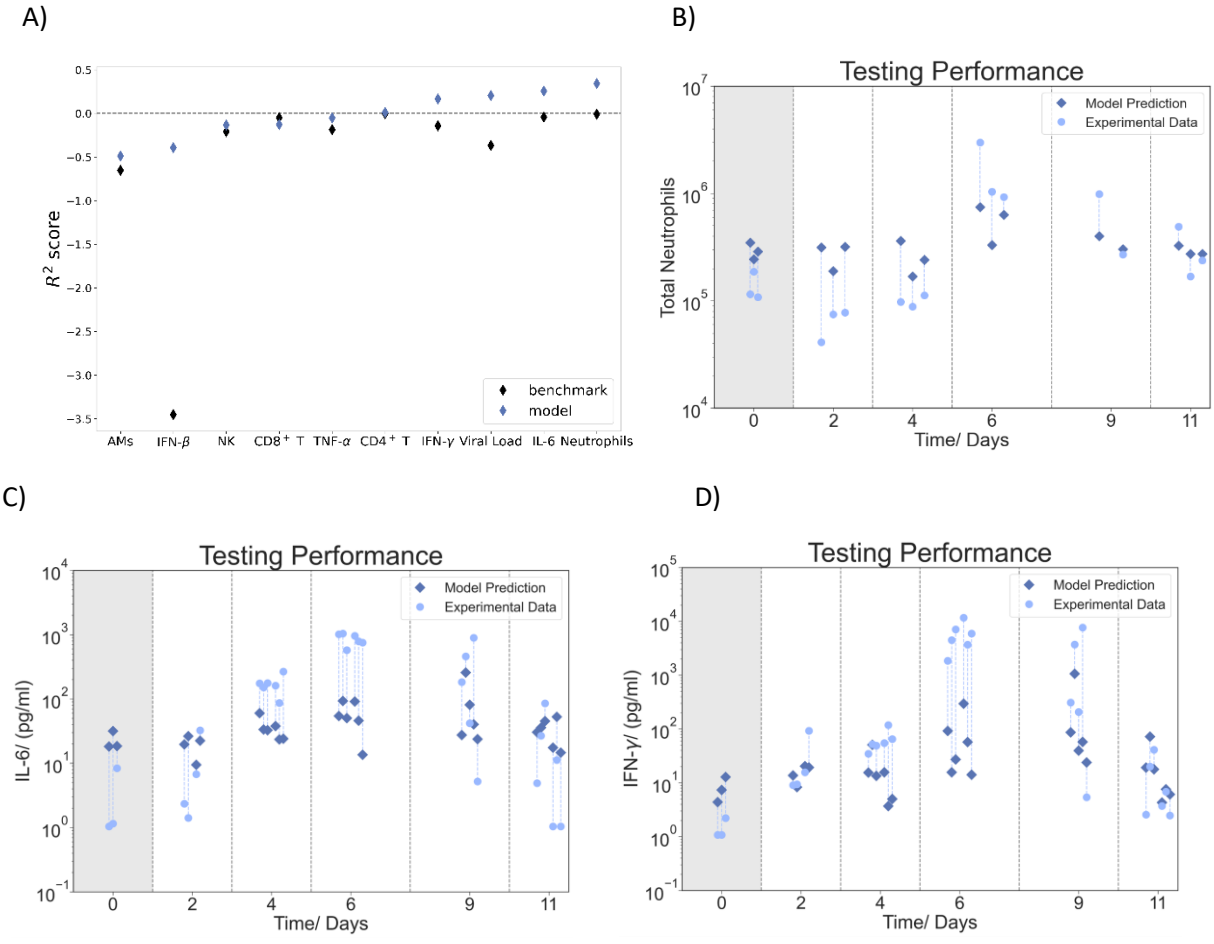

Figure 4. Summary of model predictions for various lung leukocytes and cytokines from hematological data. (A) R^2 score for different target variables. Blue diamonds show the R^2 score of the best-performing model. Black diamonds indicate the mean of the target variable obtained from the training data set and serve as a benchmark. Models that perform better than the benchmark and have a positive R^2 score indicate the model can make successful predictions. Mapping of (B) neutrophils, (C) IL-6, and (D) IFN-γ from blood data. Each blue-light circle represents one mouse, with its matching individual prediction indicated by a connected (blue dashed line) diamond. Gradient boosted regression trees and linear regression with the aid of PCA worked best for these mappings. We observed that the quality of the predictions was dependent on the stage of the infection. Neutrophils were estimated more precisely in the advanced stage of infection, while for IL-6 more accurate estimations were yielded at the peak of the infection. For complete results, please refer to the supplemental material (Supplementary Figures S13-15).

612

613 A) B)

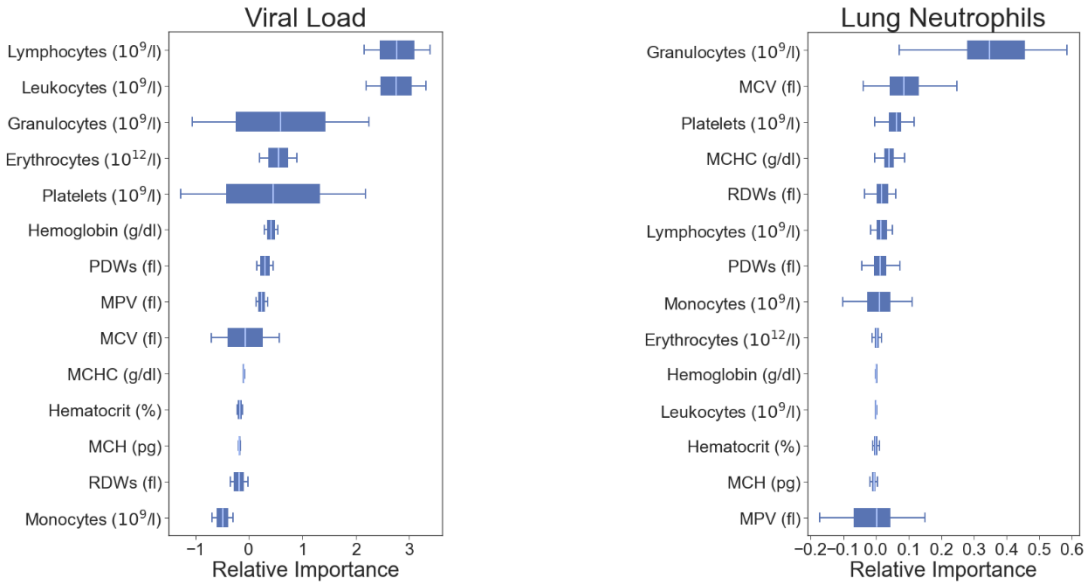

614

615 C) D)

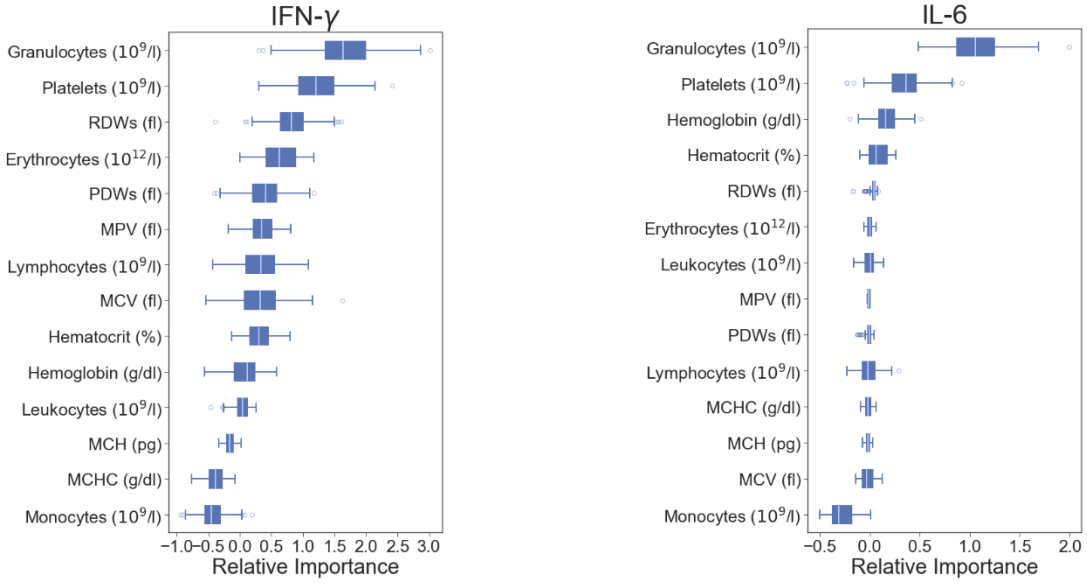

616

617 **Figure 5. Permutation importance.** The permutation importance for the mapping of (A) the viral load, (B)
618 neutrophils, (C) IFN-γ, and (D) IL-6 is indicated. We calculated the permutation importance using the
619 testing data.

TABLES

Table 1: Hematological parameters used to estimate the viral load in the lungs of mice. Blood variables are listed in order of their Pearson correlation with viral load (lowest coefficient: MCH, highest coefficient: granulocytes).

Blood variable	Interpretation
MCH (mean corpuscular hemoglobin)	average amount of hemoglobin per red blood cell
RDWs (red cell distribution width)	degree of variation in size and shape of red blood cells
Leukocytes (white blood cells)	protect against infectious diseases and foreign bodies
MPV (mean platelet volume)	average size of platelets in blood
MCV (mean corpuscular volume)	average volume of red cells
Hemoglobin	oxygen carrier in red blood cells
Erythrocytes (red blood cells)	oxygen transportation to the tissue
MCHC (MCH concentration)	concentration of hemoglobin in red blood cells per volume
Monocytes	subtype of white blood cells
PDWs (platelet distribution width)	indicates variation in platelet size
Hematocrit	volume percentage of red blood cells in blood
Lymphocytes	subtype of white blood cells
Platelets	blood component that helps stopping bleeding
Granulocytes	subtype of white blood cells

Table 2. **Best performing model and respective scores for different targets from the lung milieu.** Hematological data was used in all cases as input to the algorithms. For each target variable to estimate, different machine learning models were tested.

Target Variable	Model	MSE	R^2
Viral Load	Feedforward NN	7.53	0.18
Neutrophils	LR with PCA	0.98	0.25
IFN-γ	Feedforward NN	7.18	0.15
Interleukin-6	GBRT	4.55	0.21